A Simple Hysteretic Energy Harvesting Method for Nonneutral AC Switches in Load Automation

Karthik A and Loganathan Umanand

***Abstract*—This paper presents a simple hysteretic method to obtain the energy required to operate the gate-drive, sensors, and other circuits within nonneutral ac switches intended for use in load automated buildings. The proposed method features a switch-mode low part-count self-powered MOSFET ac switch that achieves efficiency and load current THD figures comparable to those of an externally gate-driven switch built using similar MOSFETS. The fundamental operation of the method is explained in detail, followed by the modifications required for practical implementation. Certain design rules that allow the method to accommodate a wide range of single-phase loads from 10 VA to 1 kVA are discussed, along with an efficiency enhancement feature based on inherent MOSFET characteristics. The limitations and side effects of the method are also mentioned according to their levels of severity. Finally, experimental results obtained using a prototype sensor switch are presented, along with a performance comparison of the prototype with an externally gate-driven MOSFET switch.**

***Index Terms*—Energy harvesting, floating gate-drive, load automation, self-powered switch.**

I. Introduction

ELECTRICITY is undoubtedly one of the most important forms of energy consumed today. Its utilization across the world has only increased over the years, with lighting loads contributing a major share to its consumption, especially in large buildings and public places. As with other forms of energy, electricity has often been overused, leading to the idea of its conservation by the automation of permanently connected loads using electronic switches. Methods such as wireless [1]–[3] and powerline communications [4], [5] have also been exploited in the field of load automation.

A highly desirable feature in load automation is the "nonneutral" operation of electronic load switches, allowing direct replacement of the mechanical ones, also avoiding the significant wiring that would otherwise be inevitable. However, the practical implementation of a nonneutral electronic switch presents a major challenge of obtaining a floating power supply for operating the sensors, control, communication, and gate-drive circuitry. Although such a power supply is easily obtained during the OFF-state of a switch from the voltage drop across it (using a shunt regulator etc.), providing the same during the ON-state without affecting the operation of the load, becomes quite challenging. While the use of batteries within switches present additional maintenance issues, sources such as photovoltaic cells that require a power converter and associated circuitry increase the complexity of implementation. The additional challenges presented by electronic switches concern their efficiency, performance, reliability, size, and cost that translate to lower power dissipation, improved techniques, and simple low part-count designs.

In order to circumvent the aforementioned challenges, self-powering techniques that allowed energy harvesting within electronic switches were proposed for both general [6]–[12] as well as specific applications [13], [14]. The interesting dV/dt-based self-powering method used in [6]–[8], and [13] has also been applied to ac switches [15], [16]. However, the method prohibits a static-ON operation of switches, in a similar way as the traditional bootstrap technique does, restricting the area of application to ac–ac converters. Numerous self-powered nonneutral switches reported in the past used TRIACs [5], [17]–[21] and exhibited high power losses and often distorted load current waveforms due to the use of phase control [5], [18], [19] to obtain the auxiliary power supply. Few other techniques allowed a larger voltage drop across the switch once in few cycles [22], once within a cycle [5], and for an integral number of cycles [20], thus diverting a significant amount of load current to charge a large storage capacitor, possibly affecting the normal operation of loads.

In this paper, a simple energy harvesting method that addresses the aforementioned problems is proposed for a MOSFET ac switch. The method uses the inherent characteristics of MOSFETS to harvest variable amounts of energy in several small installments over a wide range of the load current cycle, achieving both efficiency and distortion figures comparable to those of an externally gate-driven MOSFET switch. Further, the proposed method is also self-oscillating and, thus, completely avoids the use of a separate modulator circuit.

II. Proposed Energy Harvesting Method

Fig. 1(a) shows a MOSFET in its ON-state being gate-driven by a boost converter that is, in turn, powered from the voltage drop across the MOSFET ($V_{\rm DS}$), yielding a self-powered dc switch. The voltage source $V_{\rm ADJ}$ enables the adjustment of the peak input current of the boost converter.

Fig. 1(a) also shows a resistor $R_{\rm bleed}$ across the output of the boost converter that represents the real power consumed by auxiliary loads, like sensors, wireless modules, etc., powered within the switch. A minimum voltage equal to V_T, the threshold voltage of the MOSFET, is thus available for these loads. If desired, further regulation may be applied to this local power

Manuscript received October 24, 2014; revised July 27, 2015; accepted September 15, 2015. Date of publication September 22, 2015; date of current version January 28, 2016. Recommended for publication by Associate Editor C. Fernandez.

The authors are with the Center for Electronics Design and Technology, Indian Institute of Science, Bangalore 560012, India (e-mail: akarthik@cedt.iisc.ernet.in; lums@cedt.iisc.ernet.in).

Digital Object Identifier 10.1109/TPEL.2015.2480873

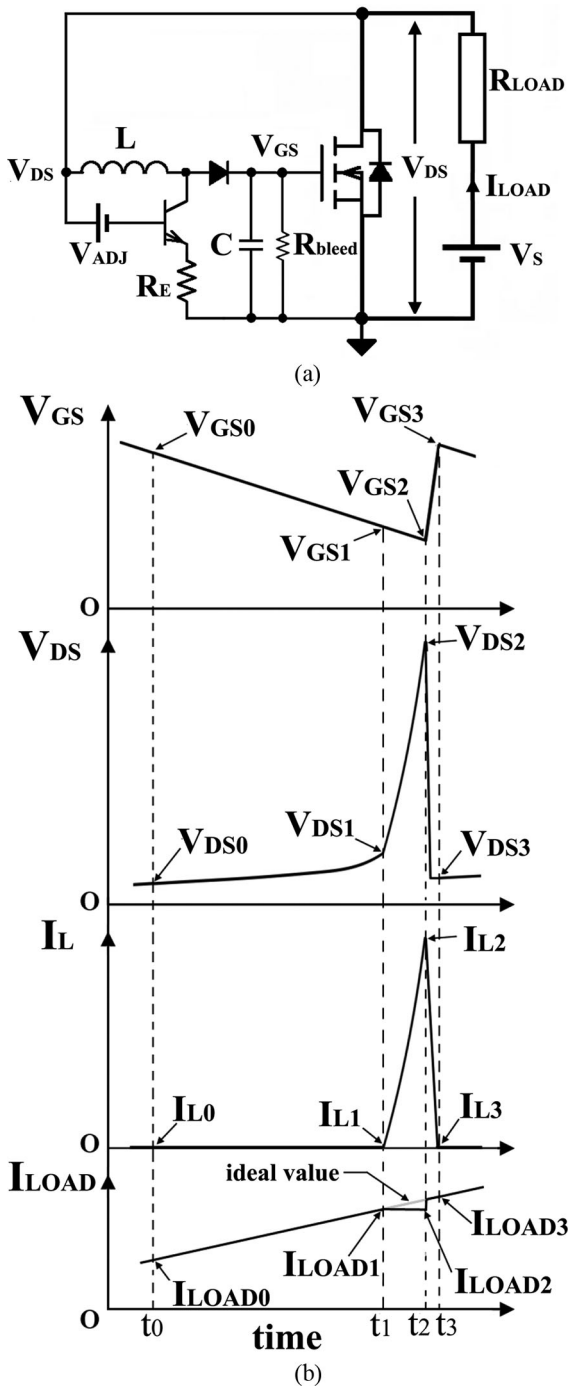

Fig. 1. (a) Proposed energy harvesting method applied to a MOSFET. (b) Relevant waveforms for a switching cycle of operation.

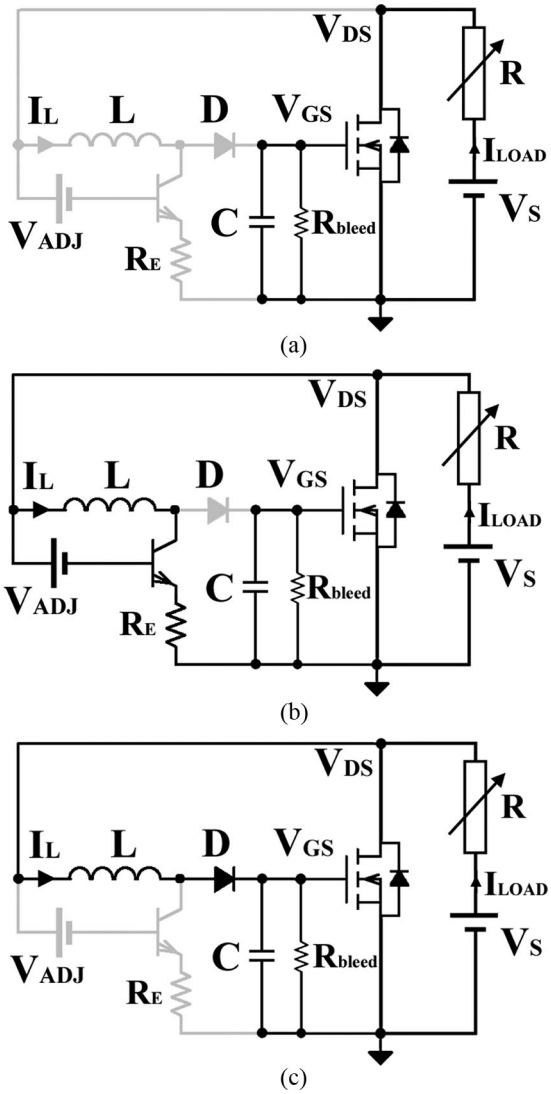

Fig. 2. Operation of the proposed energy harvesting circuit. (a) Operation during the time interval t_0–t_1. (b) Operation during the time interval t_1–t_2. (c) Operation during the time interval t_2–t_3.

supply by means of a low dropout or a shunt regulator. Negative power supplies may also be obtained from the proposed energy harvesting circuit as shown in Fig. 3(b).

A. Operation of the Proposed Method

Fig. 1(b) shows the relevant waveforms for the operation of the proposed method. In order to explain the details of operation, a switching cycle is divided into three time intervals.

1) Time Interval 1 (t_0–t_1): At t_0, it is reasonably assumed that the capacitor C is charged to $V_{GS0} > V_{DS0} + V_T$, indicating that the MOSFET is in its linear region. The inductor current I_{L0} is zero and the drain current I_D equals the load current I_{LOAD}, giving the voltage drop across the MOSFET as

$$V_{\mathrm{DS0}} = I_{D0} R_{\mathrm{DS}} = I_{\mathrm{LOAD0}} R_{\mathrm{DS}}. \tag{1}$$

The capacitor C discharges through R_{bleed} in an exponential manner, approximated by (2), for a typically large time constant $R_{\mathrm{bleed}}C$

$$V_{\mathrm{GS}} = V_{\mathrm{GS0}} \left(1 - \frac{t}{R_{\mathrm{bleed}}C}\right). \tag{2}$$

At t_1, V_{rmGS} reduces to V_{GS1}, causing V_{DS} to slightly rise to V_{DS1}, beyond which, the MOSFET slips into the saturation region, exhibiting a substantially higher voltage gain ($\frac{\Delta V_{\mathrm{DS}}}{\Delta V_{\mathrm{GS}}}$).

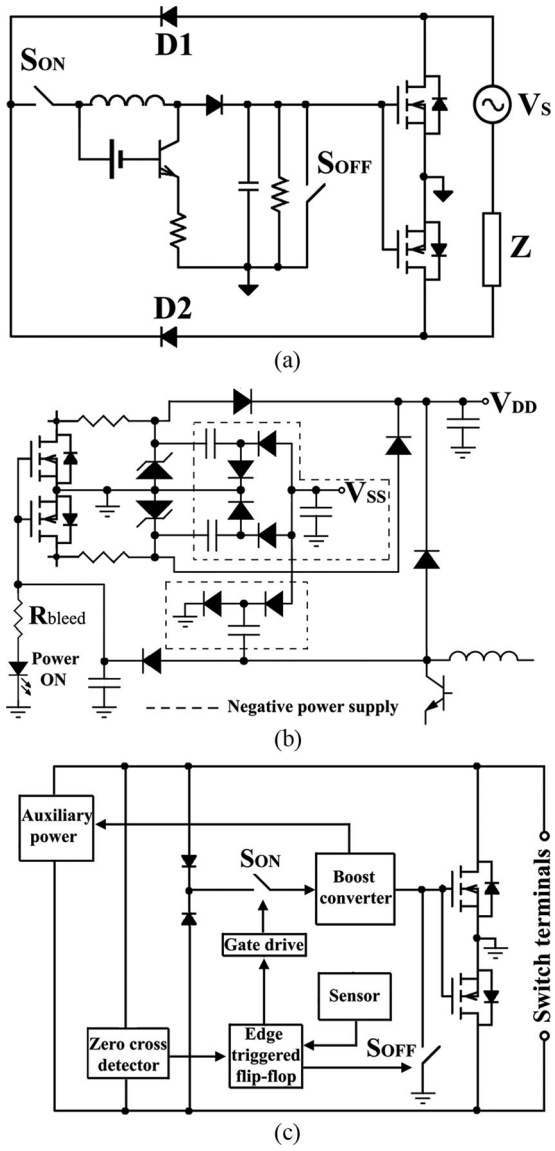

Fig. 3. Modifications for practical application of the proposed method. (a) Proposed circuit modified for ac applications. (b) Generation of auxiliary power supplies within the switch. (c) Block schematic of the proposed switch.

This value of $V_{\rm DS}$ is given as

$$V_{\rm DS1} = V_{\rm GS1} - V_T. \tag{3}$$

Fig. 2(a) highlights the portion of the circuit that is operational during this time interval. It may be noted that the inductor current I_L is zero throughout the time interval as V_{DS} being small is unable to turn on the boost transistor.

2) Time Interval 2 (t_1–t_2): As the capacitor *C* continues to discharge toward V_{GS2}, the MOSFET (which is now in saturation) amplifies the downward variation in the gate voltage V_{GS}, enhancing V_{DS} to reach $V_{DS2} = V_{\rm DS,max}$ at t_2. Meanwhile, the inductor current I_L rises to attain its peak value $I_{L2} = I_{L,\rm max}$, given as

$$I_{L,\rm max} = \frac{V_{\rm DS,max} - V_{\rm ADJ} - V_{\rm BE,cut}}{R_E}. \tag{4}$$

TABLE I
ON AND OFF STATES OF THE BIDIRECTIONAL SWITCH FOR COMBINATIONS OF S_{ON} AND S_{OFF}

S_{ON}	S_{OFF}	Four-quadrant switch
ON	OFF	Conduction (ON)
OFF	ON	Blocking (OFF)

Because of the nonzero inductor current for this time interval, the actual load current $I_{\rm LOAD}$ is less than the ideal load current as shown in Fig. 1(b). The operational parts of the circuit during this interval are emphasized in Fig. 2(b).

3) Time Interval 3 (t_2–t_3): As I_L reaches $I_{L,\rm max}$ at t_2, the voltage drop across R_E is sufficient to turn off the transistor, forcing the inductor to transfer its energy to the capacitor *C*. Meanwhile, $V_{\rm DS}$ falls rapidly, owing to the high voltage gain of the MOSFET in the saturation region. At t_3, the energy transfer from the inductor to the capacitor is complete and I_L has fallen back to zero. The gate voltage has risen to $V_{\rm GS3}$, and the MOSFET is once again in its linear region, with a voltage drop across its channel given by

$$V_{\rm DS3} = I_{D3} R_{\rm DS} = I_{\rm LOAD3} R_{\rm DS}. \tag{5}$$

This time interval completes one cycle of operation. Fig. 2(c) shows the circuit activity for this time interval.

B. Modifications Required for Practical Application

1) Extension to AC Switches: The proposed method may be extended to control two MOSFETS in a four-quadrant configuration (for ac applications) with the addition of two rectifier diodes D1 and D2 as shown in Fig. 3(a). However, it is worth noting that only the forward-conducting MOSFET moves into saturation during recharge periods, while the other MOSFET remains entirely in its linear region performing synchronous rectification and, thereby, reducing the conduction losses within the switch.

2) ON/OFF Operation: While the ac switch is turned OFF by breaking the energy flow to the boost converter followed by a gate discharge of the MOSFETS, restoring the energy flow turns it ON. For this purpose, two static switches S_{ON} and S_{OFF} that operate complementarily are included as shown in Fig. 3(a). Table I lists the ON/OFF positions of the four-quadrant switch for the two valid combinations of S_{ON} and S_{OFF}. It may be noted that S_{ON} is a high-voltage low-current device, and S_{OFF} is a low-voltage device with a high peak current capability.

It is highly desirable that the OFF-to-ON and ON-to-OFF state transitions of an ac switch be carried out at zero-crossing instants of the mains voltage and the load current, respectively [17]. This zero-crossing timing information is easily obtained by comparing the voltages across the two MOSFETS (w.r.t. ground) against each other. An advantage of such a comparison is that it may be used irrespective of the ON or OFF condition of the switch. The output of the comparison may be used to clock an edge-triggered flip-flop, thereby synchronizing the state changes of the switch to the zero-crossing moments.

3) Powering of Sensors and Auxiliary Loads: As already mentioned in Section II, any auxiliary power supplies (for the

operation of S_{ON}, S_{OFF}, zero-crossing detector, sensor, etc.) can be obtained from the gate(s) of the MOSFETS during the ON state of the switch. However, during the OFF state, a second power supply, derived from the mains voltage blocked across the switch, needs to be used to provide auxiliary power as shown in Fig 3(b). It is worth noting that the self-oscillating capability of the proposed method enables charge pumps to be driven, thereby simplifying the synthesis of negative power supplies. Moreover, the resistor $R_{\rm bleed}$ may also be used in series with an LED [see Fig. 3(b)] to obtain a power-ON indication feature. Based on the above modifications, a block schematic for the proposed switch is shown in Fig. 3(c).

C. Oscillation Criteria and Minimum Load Current Limit

In the modified circuit shown in Fig. 3(a), when the peak load current is less than the peak inductor current $I_{L,\max}$, the boost transistor never turns off, thus conducting the entire load current through it. The system, thus, fails to oscillate and/or harvest energy as the gate voltage V_{rmGS} remains below the threshold voltage V_T, and $V_{\rm DS}$ is also too small to provide any self-powering action. If V_D, represents the forward drop of a diode, the value of $V_{\rm DS,max}$ at the verge of oscillation (i.e., at $V_{\rm GS,max} = V_T$) satisfies (6). Since this value of $V_{\rm DS,max}$ also coincides with the turn-off of the boost transistor, the required value for $V_{\rm ADJ}$ may be obtained as

$$V_{\rm DS,max} = V_{\rm GS,max} + 2V_D = V_T + 2V_D \tag{6}$$

$$V_{\rm DS,max} = I_{L,\max}R_E + V_{\rm BE,cut} + V_{\rm ADJ} + V_D \tag{7}$$

$$V_{\rm ADJ} = V_T + V_D - V_{\rm BE,cut} - I_{L,\max}R_E. \tag{8}$$

Thus, the peak inductor current $I_{L,\max}$ is a design parameter that needs to be chosen less than or equal to the minimum load current specification so as to ensure oscillations (and energy harvesting) at the lightest load conditions.

However, since sustained oscillations are a result of two opposite system states endlessly supporting each other, it is also necessary that the energy released by the inductor $E_{\max}$ results in a value of $V_{\rm GS,max}$ that is large enough to enhance the MOSFETS and reduce $V_{\rm DS}$ to a small value. Thus, the minimum value for the boost inductor required to sustain oscillation is obtained as

$$E_{\max} = \frac{1}{2}LI_{L,\max}^2 > \frac{1}{2}C_{\rm eq}(V_{\rm GS,max}^2 - V_T^2) \tag{9}$$

$$L > C_{\rm eq}\frac{V_{\rm GS,max}^2 - V_T^2}{I_{L,\max}^2}. \tag{10}$$

In the above expression, $C_{\rm eq}$ is the effective value of the capacitor C and the gate capacitances of the MOSFETS. It may be noted that the inductance value given by the above expression needs to be exceeded by a sufficient margin to accommodate all the auxiliary circuits powered within the switch.

D. Enhancement of Efficiency at Heavy Load Currents by Variation of Switching Frequency

At the boundary between the linear and saturation regions of a MOSFET, the relation between its gate voltage and drain current is given by

$$(V_{\rm GS} - V_T) \propto \sqrt{I_D}. \tag{11}$$

In Fig. 1(b), at t_1, V_{rmGS} falls to $(V_{\rm DS} + V_T)$, which may be approximated as its minimum value $V_{\rm GS,min}$, since further reduction in V_{rmGS} during the time interval (t_1–t_2) is small. The drain current I_D is the load current $I_{\rm LOAD}$, as the inductor current I_L at t_1 is zero. Thus, (11) may be rewritten as follows:

$$V_{\rm GS,min} \propto \sqrt{I_{\rm LOAD}}. \tag{12}$$

During the time interval (t_1–t_2), when the MOSFET behaves as an inverting amplifier, the variation in $V_{\rm GS,min}$ with load current over several switching cycles is also followed by $V_{\rm DS,max}$, $I_{L,\max}$, and $E_{\max}$ according to (7) and (9). Thus, the amount of energy harvested in a switching cycle increases with load current, leading to longer discharge times and reduced switching frequency. It is the advantage of this reduction in switching frequency that forms the basis for improved efficiencies at higher load currents by reducing the power dissipated in the switch.

E. Fault Detection and Protection

Electronic switches may be protected against damage due to an overload or a short-circuit condition that is usually detected by sensing the voltage drop across the switch. Considering the operation of the proposed method that gives rise to recharge spikes across the switch, it may, at first, seem to be almost impossible to implement a protection scheme for the same. However, a fault condition may still be sensed across the reverse-conducting (synchronous) MOSFET that is operated entirely in its linear region, without any recharge spikes across it.

In the event of a short-circuit, the body diode clamps the voltage drop across the synchronous MOSFET (to about 1 V), providing the necessary trip voltage for detection by the protection circuitry. However, normal operation implies that the values of $I_{\rm LOAD}R_{\rm DS}$ is lesser than the nominal body diode drop, resulting in synchronous rectification. It may be noted that the aforementioned method senses the trip voltages for the two half-cycles separately that need to be combined before being compared to a threshold. A suitable blanking time may also be used to avoid false tripping due to transients.

III. Limitations and Side Effects

Although switch-mode operation forms the basis for the energy harvesting capability of the method, it also gives rise to few limitations and side effects. These are briefly described in this section in the order of decreasing severity.

A. Restrictions on Load Type

Power conversion at a nonconstant frequency causes high-frequency (HF) components distributed over a wide band of frequencies. Similarly, in the proposed method, wideband HF components are injected into the grid depending on the nature of the connected load.

The power quality for resistive and inductive loads is excellent, as they exhibit large impedances at HF. However, capacitive

loads permit spikes in the load current, also reducing the reliability of the MOSFETS. Therefore, it is not recommended (although possible) to operate capacitive (and nonlinear) loads using the proposed self-powering method.

B. Additional Losses Incurred by the Devices

Since the proposed energy harvesting method involves frequent saturation of the MOSFETS, additional switching losses are incurred by them, reducing the overall efficiency of the switch. These losses also give rise to ripple in the junction temperatures of the devices. A practical evaluation of efficiency and junction temperature ripple caused by the switching action is given in Section IV-B.

C. Effects of Temperature Variation

There are two heating mechanisms within the proposed self-powered switch namely, the conduction and the switching losses. Higher temperatures cause a rise in the $R_{\rm DS}$ of the MOSFETS increasing the conduction losses. However, variations in switching losses are minimal, owing to the positive and negative temperature coefficients of voltage gain ($\frac{\Delta V_{\rm DS}}{\Delta V_{\rm GS}}$) and threshold voltage V_T, respectively, that prevent runaway of switching frequency. This fact has also been substantiated by experimental results [see Figs. 4(a) and 5(b)] in the next section of this paper. Meanwhile, the effect of temperature on the boost transistor and other components may be safely neglected, as they conduct much lesser currents compared to the MOSFETS.

D. Load Current Distortion

In the proposed method, the deviation of load current from its ideal value [see Fig. 1(b)] during harvesting intervals contributes to its distortion. However, by choosing an appropriate value for $I_{L,\max}$ (considering the minimum load current), it is possible to keep the distortion close to that of an externally gate-driven MOSFET switch. This has been experimentally verified in Section IV-B.

IV. Experimental Results

In order to confirm the feasibility of the proposed method, a prototype switch (see Fig. 7) of the following specifications was built and tested.

Mains voltage: 250-V ac, 50 Hz.
Load current range: 50 mA to 5 A (10 VA to 1 kVA).
MOSFETS: SPW47N60C3 [23].
Auxiliary Load: TSOP34838 38-kHz IR sensor.

The experimental results obtained using the same, from the perspectives of both functionality as well as performance, have been presented in this section. The inductor value was adjusted to provide a switching frequency close to 1 kHz at maximum load current and the minimum peak inductor current $I_{L,\max}$ was 50 mA. The value for $V_{\rm ADJ}$ was 3 V, obtained by the diode connection of an IRFZ44 MOSFET. The resistors R_E and $R_{\rm bleed}$ were at 22 Ω and 3.3 kΩ, respectively, with an LED in series with $R_{\rm bleed}$, for power-on indication.

A. Functionality

The oscillograms recorded during the ON-state of the proposed switch for resistive loads of value 50 Ω (max. load) and 5 kΩ (min. load) are shown in Fig. 4. The switch drop for 50-Ω load [see Fig. 4(a)] exhibits a distinct sinusoidal portion of 1.65 $V_{\rm pp}$ with occasional recharge spikes reaching 10 V at a switching frequency close to 1 kHz. This waveform clearly depicts the superiority of the proposed method over TRIACs of similar die sizes that exhibit sinusoidal voltage drops around 4 $V_{\rm pp}$. The gate-drive voltage V_{rmGS} [see Fig. 4(c)] is hysteretically regulated to 4.5 V ± 1 V, with $V_{\rm GS,min}$ following the square root of the load current as mentioned in Section II-C. The auxiliary power supply of 4.8 V, as shown in Fig. 4(e), also receives a tight regulation of ±200 mV.

On the other hand, the switch drop for a 5-kΩ (min.) load [see Fig. 4(d)] exhibits an almost rectangular envelope due to the operation of the MOSFET in the cutoff ($V_{rmGS} < V_T$) and weak saturation ($V_{rmGS} \approx V_T$) regions as the $I_{\rm LOAD}$ rises from zero. Oscillations begin when $I_{\rm LOAD}$ meets $I_{L,\max}$ at approximately 2.5 ms from the zero crossing and harvest energy for another 5 ms of the half cycle, periodically driving the MOSFET into the linear region. Recharge spikes peak at 4 V with a switching frequency of approximately 5 kHz. $V_{\rm GS,max}$ [see Fig. 4(d)] touches the threshold voltage V_T ($\approx$ 2.4 V) during the oscillations as mentioned in Section II-C. Meanwhile, the auxiliary supply [see Fig. 4(f)] is maintained at 2.9 V ± 200 mV.

Fig. 5(a) shows the voltage developed across a 5-kΩ load during the OFF-state of the switch due to its leakage current that amounts to approximately 2 mA. It is worth noting that the leakage currents of MOSFETS are only a few hundreds of nanoamperes, but with the addition of the OFF-state power supplies and protection features, like snubbers, TVS diodes, etc., a higher net leakage results through the switch.

The effect of temperature on the operation of the proposed circuit, as mentioned in Section III-C, is also verified in this section. The voltage drop across the prototype switch at a MOSFET case temperature of 90 °C is shown in Fig. 5(b).

The waveform shows the sinusoidal portion of the waveform having increased to 2.75 $V_{\rm pp}$ compared to 1.65 $V_{\rm pp}$ at 30 °C [see Fig. 4(a)] indicating a 66% rise in the channel resistance ($R_{\rm DS}$) of the MOSFETS. However, the recharge spikes and switching frequency are more or less the same as in Fig. 4(a), proving the robustness of the proposed method against higher temperatures.

The prototype switch was also tested for zero-crossing timing, by using an IR remote control to turn it ON and OFF, while driving a 50-Ω load. The experimental results for the same are shown in Fig. 5(c) and (d) to sum up the basic functionality testing of the prototype switch.

B. Performance

In order to evaluate the performance of the prototype switch, it was compared with an externally gate-driven reference switch [see Fig. 6(a)] that used similar MOSFETS. The comparison was made in terms of two main parameters namely efficiency and load current THD. Both the prototype and the reference switches were tested for a 50-Ω load under the same grid conditions, while

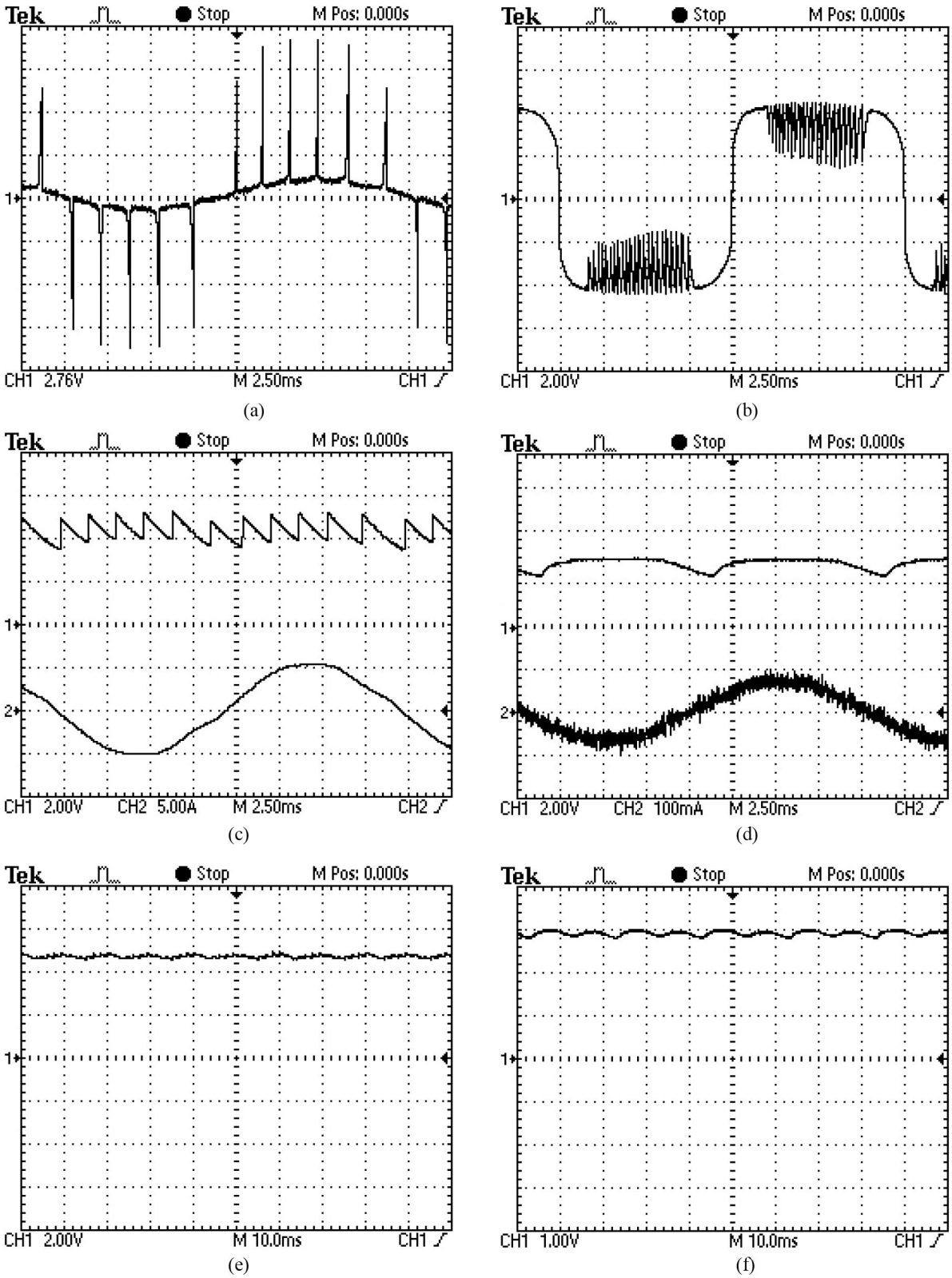

Fig. 4. Experimental waveforms for ON-state drop, gate-drive voltage, and load current for (a), (c), (e) 50-Ω (max.) load and (b), (d), (f) 5-kΩ (min.) load. (a) Voltage drop across the switch; (Scale: *X*-axis: 2.5 ms/div, *Y*-axis: 2.76 V/div). (b) Voltage drop across the switch; (Scale: *X*-axis: 2.5 ms/div, *Y*-axis: 2 V/div). (c) (1) Gate–source voltage V_{GS} ; (Scale: *X*-axis: 2.5 ms/div, *Y*-axis: 2 V/div), (2) Load current (Scale: *X*-axis: 2.5 ms/div, *Y*-axis: 5 A/div). (d) (1) Gate–source voltage V_{GS}; (Scale: *X*-axis: 2.5 ms/div, *Y*-axis: 2 V/div), (2) Load current (Scale: *X*-axis: 2.5 ms/div, *Y*-axis: 100 mA/div). (e) Auxiliary supply voltage in case of a 50-Ω load; (Scale: *X*-axis: 10 ms/div, *Y*-axis: 2 V/div). (f) Auxiliary supply voltage in case of a 5-kΩ load; (Scale: *X*-axis: 10 ms/div, *Y*-axis: 1 V/div).

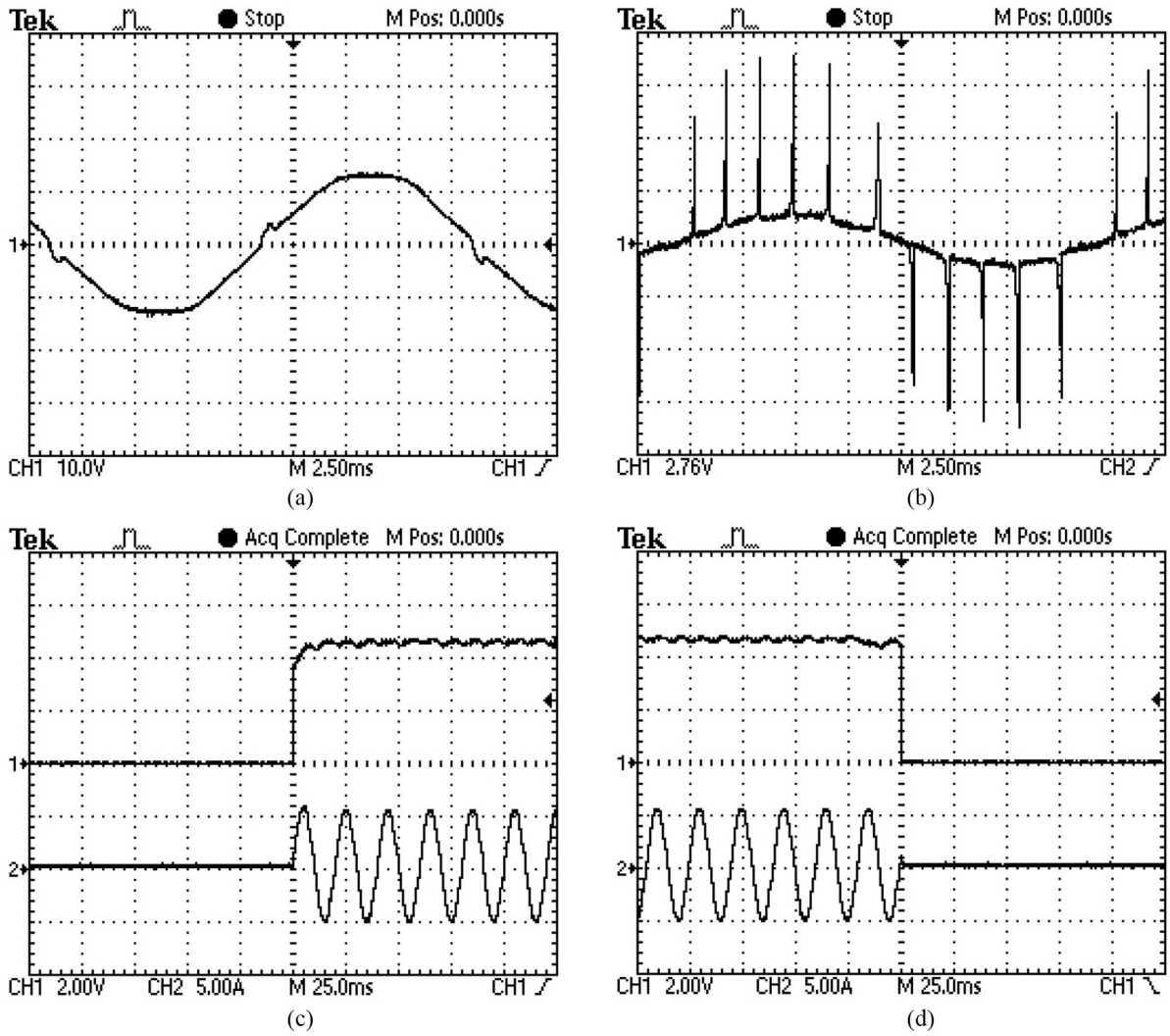

Fig. 5. (a) Leakage performance. (b) Effect of higher temperatures on the operation of the switch. (c) and (d) Transitions from OFF to ON and vice versa. (a) Experimental result for voltage drop across a load resistance of 5 kΩ due to the OFF-state leakage current; (Scale: *X*-axis: 2.5 ms/div, *Y*-axis: 10V/div). (b) Voltage drop across the switch at a case temperature of 90 °C for 50-Ω load; (Scale: *X*-axis: 2.5 ms/div, *Y*-axis: 2.76 V/div). (c) Zero-voltage turn-on for a 50-Ω load; (1) turn-on logic signal (Scale: *X*-axis: 25 ms/div, *Y*-axis: 2 V/div), (2) load current (Scale: *X*-axis: 25 ms/div, *Y*-axis: 5 A/div). (d) Zero-current turn-off for a 50-Ω load; (1) turn-on logic signal (Scale: *X*-axis: 25 ms/div, *Y*-axis: 2 V/div), (2) load current (Scale: *X*-axis: 25 ms/div, *Y*-axis: 5 A/div).

the latter was fed with a gate–source voltage (V_{rmGS}) of 12 V [see Fig. 6(a)]. The results of the comparison are presented in this section.

1) Efficiency: Fig. 6(c) and (e) shows the product of switch drop and load current (obtained using the MATH function on the oscilloscope) for the reference and prototype switches, respectively. The average values of these waveforms directly give the total losses incurred by the reference and prototype switches as 2.04 and 3.36 W, respectively. Based on the nominal load power of 1 kW, the efficiencies for the reference and the prototype switches are obtained as 99.66% and 99.79%, respectively, indicating the comparability of performance to each other.

2) Junction Temperature Rise due to Pulsed Power Losses: Fig. 6(c) and (e) shows more or less similar wave shapes for the reference and prototype switches, except for the recharge spikes in the latter that are responsible for the additional losses incurred by it. Although the average additional loss is small, the high peak losses possibly cause a ripple in the junction temperatures of the MOSFETS [24] that needs to be minimal so as to ensure device reliability. Fig. 6(b) shows a time expansion of the power loss waveform in Fig. 6(e) around the 5 ms instant (from the zero crossing) when the highest pulsed power is incurred by the switch. This rise in junction temperature due to the presence of pulses may now be estimated using the following parameters [24].

Equivalent rectangular pulse width [see Fig. 6(b)]: 100 μs.
Peak nonpulsed power loss [see Fig. 6(b)]: 4 W.
Additional pulse power [see Fig. 6(b)]: $53.2-4 = 49.2$ W.
Average switching period [see Fig. 5(b)]: 1.75 ms.

Assuming a triangular power-loss pulse curve [see Fig. 6(b)] gives an effective duty cycle of 0.057, leading to a worst-case additional power loss of 2.8 W due to the pulsed operation. Considering the thermal impedance ($Z_{\mathrm{th-jc}}$) of 0.04 °C/W from

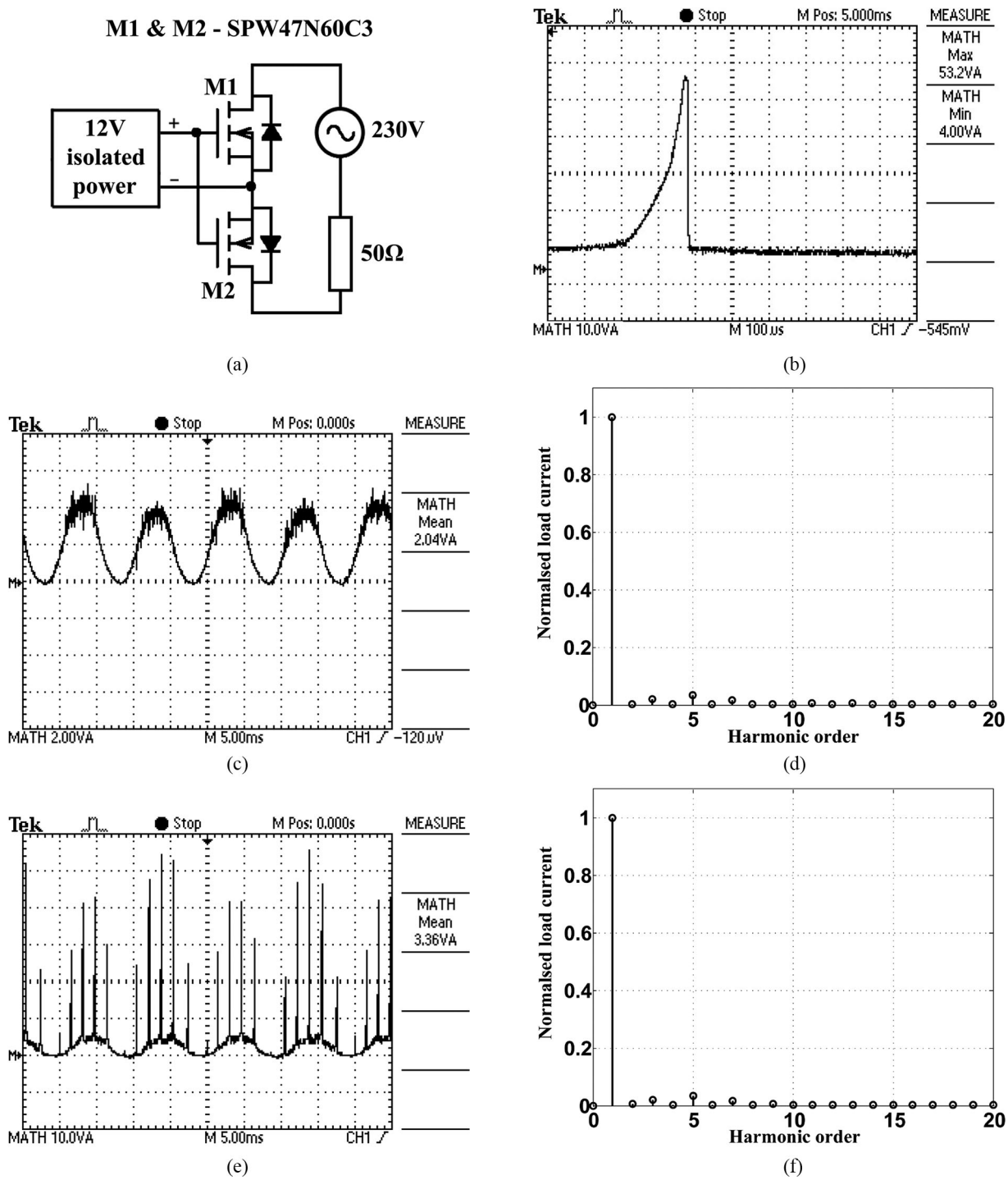

Fig. 6. Performance comparison of the prototype and the externally gate-driven reference MOSFET switches. (a) Circuit schematic for the externally gate-driven reference MOSFET switch used for performance comparison. (b) Peak pulsed power loss incurred by the proposed switch; (Scale: *X*-axis: 100 μs/div, *Y*-axis: 10 W/div). (c) Product of voltage drop and load current waveforms for the reference switch; (Scale: *X*-axis: 5 ms/div, *Y*-axis: 2 W/div). (d) Normalized FFT spectrum of the load current through the reference switch. (e) Product of voltage drop and load current waveforms for the prototype switch; (Scale: *X*-axis: 5 ms/div, *Y*-axis: 10 W/div). (f) Normalized FFT spectrum of the load current through the prototype switch.

junction to case [23], the estimated junction temperature rise due to the pulse is 1.97 °C, which is close to the product of the averaged pulsed power and thermal resistance ($R_{\mathrm{th-jc}}$) at 0.84 °C. However, both these values being quite negligible compared to the normal operating junction temperature range of 350 to 400 K (75 to 125 °C), it may be concluded that the thermal stress caused by pulsed operation is indeed harmless to the reliability of the MOSFETS.

3) Load Current Distortion: A comparison of distortion performance of the prototype and reference switches was carried

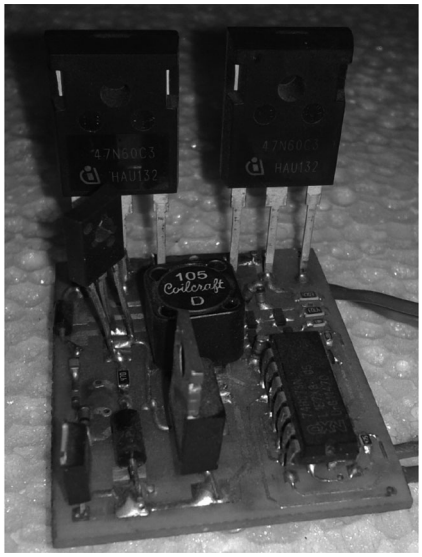

Fig. 7. Photograph of the prototype switch used for testing.

TABLE II
COMPARISON OF SELF-POWERING/ENERGY HARVESTING TECHNIQUES

Aspect	Proposed method	Methods in [3], [5], [17]–[19], [21]	Method in [15] and [16]
Device(s)	MOSFET	TRIAC	MOSFET
Static-ON	Yes	Yes	No
Resistive load	Yes	Yes	Yes
Inductive load	Yes	[5]—No	Yes
Capacitive load	Yes, but not recommended	[5]—Yes	Not recommended
Nonlinear load	Yes, but not recommended	No	Not recommended
Min. load current limit	By design	Holding current	No nonneutral operation
Voltage drop	Low	High	Possibly low
Load current distortion	Low	[5], [18], [19]—high [3], [17], [21]—low	Low
Leakage current	Low	Possibly high (TRIAC)	Low
Zero-voltage turn-on	Yes	[5], [17]—Yes	Possible
Zero-current turn-off	Yes	[17]–[19]—Yes	Possible

out using the normalized FFT spectra [see Fig. 6(f) and (d)] of the respective load currents. The corresponding THD figures were obtained as 4.37% and 4.40%, indicating their equivalence in terms of load current fidelity. It may be noted that this method of comparison is used in order to eliminate the effects of a distorted mains voltage waveform.

V. QUALITATIVE COMPARISON WITH OTHER AC SWITCHES

Table II presents a qualitative comparison of the proposed method with the few existing self-powered ac switches. The proposed method is capable of static-ON, nonneutral operation of the switch, low leakage current, and zero-crossing features relevant to the area of load automation. The method also achieves reduced losses and distortion due to the variable switching frequency technique based on the inherent characteristics of MOSFETS.

VI. CONCLUSION

In this paper, an improved and simple energy harvesting method was proposed for a MOSFET-based ac switch, intended for use with single-phase domestic loads in load automated buildings. The proposed method allowed a self-powered switch to obtain efficiency and THD figures comparable to those achieved by an externally gate-driven MOSFET switch. The method focused on harvesting energy throughout the load current cycle in a hysteretic manner results in lower distortion of the load current. The modifications required for practical application of the method were explained with relevant circuit and block level diagrams. Certain design rules for obtaining the required operational load range and maintaining oscillations were discussed in detail, followed by an explanation of an efficiency enhancement strategy at heavy load currents, based on the inherent MOSFET characteristics. Certain limitations and side effects of the proposed method were also mentioned. Finally, experimental results obtained using a laboratory prototype incorporating the proposed method were presented along with a performance comparison of the prototype with an externally gate-driven MOSFET ac switch, so as to confirm its feasibility in terms of both functionality as well as performance.

REFERENCES

[1] N. Langhammer and R. Kays, "Performance evaluation of wireless home automation networks in indoor scenarios," *IEEE Trans. Smart Grid*, vol. 3, no. 4, pp. 2252–2261, Dec. 2012.
[2] C. Gomez and J. Paradells, "Wireless home automation networks: A survey of architectures and technologies," *IEEE Commun. Mag.*, vol. 48, no. 6, pp. 92–101, Jun. 2010.
[3] J. M. Moskin, "Two-terminal line-powered control circuit," U.S. Patent 4 678 985, Jul. 7, 1987.
[4] N. R. James, A. Eldhose, and D. D. Krishna, "PLC modem for home automation over three phase power line," in *Proc. 4th Int. Conf. Comput. Commun. Netw. Technol.*, Jul. 4–6, 2013, pp. 1–4.
[5] D. A. Lech, "Trickle power supply," U.S. Patent 5 907 198 A, May 25, 1999.
[6] R. Mitova, J. C. Crebier, L. Aubard, and C. Schaeffer, "Fully integrated gate drive supply around power switches," *IEEE Trans. Power Electron.*, vol. 20, no. 3, pp. 650–659, May 2005.
[7] J.-C. Crebier and N. Rouger, "Loss free gate driver unipolar power supply for high side power transistors," *IEEE Trans. Power Electron.*, vol. 23, no. 3, pp. 1565–1573, May 2008.
[8] N. Rouger, J.-C. Crebier, R. Mitova, L. Aubard, and C. Schaeffer, "Fully integrated driver power supply for insulated gate transistors," in *Proc. IEEE Int. Symp. Power Semicond. Devices and IC's*, 2006, pp. 1–4.
[9] H. Wang and F. Wang, "A self-powered resonant gate driver for high power MOSFET modules," in *Proc. IEEE Appl. Power Electron. Conf.*, 2006, pp. 183–188.
[10] D. Peftitsis, J. Rabkowski, and H. -P. Nee, "Self-Powered gate driver for normally-ON SiC JFETs: Design considerations and system limitations," *IEEE Trans. Power Electron.*, vol. 29, no. 10, pp. 5129–5135, Oct. 1, 2014.
[11] D. Peftitsis, J. Rabkowski, and H.-P. Nee, "Self-powered gate driver for normally silicon carbide junction field-effect transistors without external power supply," *IEEE Trans. Power Electron.*, vol. 28, no. 3, pp. 1488–1501, Mar. 2013.
[12] N. Rouger and J.-C. Crebier, "Toward generic fully integrated gate driver power supplies," *IEEE Trans. Power Electron.*, vol. 23, no. 4, pp. 2106–2114, Jul. 2008.
[13] N. Rouger, J.-C. Crebier, and S. Catellani, "High efficiency and fully integrated self powering technique for intelligent switch based flyback converters," *IEEE Trans. Ind. Appl.*, vol. 44, no. 3, pp. 826–835, May 2008.

[14] M. H. Vafaie, E. Adib, and H. Farzanehfard, "A self powered gate drive circuit for tapped inductor buck converter," in *Proc. 3rd Power Electron. Drive Syst. Technol. Conf.*, Feb. 15–16, 2012, pp. 379–384.
[15] B. Nguyen-Dac, J. C. Crebier, R. Mitova, L. Aubard, and C Schaeffer, "AC switches with integrated gate driver supply," in *Proc. Eur. Conf. Power Electron. Appl.*, Dresden, Germany, Sep. 11–14, 2005, pp. 1–9.
[16] J. C. Crebier and B. D. Nguyen, "Gate drive supplies and dead time management circuit for AC to AC converters," *IEEE Trans. Power Electron.*, vol. 25, no. 1, pp. 168–177, Jan. 2010.
[17] R. H. Forrest, "Electronic switching circuits," U.S. Patent US3 881 118, Apr. 29, 1975.
[18] R. Goldstein, "Power supply and control circuit for series connected controller," U.S. Patent 4 274 045, Jun. 16, 1981.
[19] W. W. Evans, "Self-powered, self-regulated, electronic AC control system," U.S. Patent 4 504 778 A, Mar. 12, 1985.
[20] D. Bensoussan and D. Tardio, "Means for refreshing a triac control circuit power supply," U.S. Patent 5 025 134 A, Jun. 18, 1991.
[21] L. Pelletier and A. Delaporte, "Method and apparatus for generating a supply voltage necessary for the operation of an electronic switch," U.S. Patent 6 690 150 B2, Feb. 10, 2004.
[22] B. B. Jensen and K. I. McCavit, "Direct current power supply for use in series with a load in an alternating current circuit," U.S. Patent 5 600 552 A, Feb. 4, 1997.
[23] Infineon Technologies AG, "CoolMOS power transistor datasheet for SPW47N60C3," Nov. 2, 2008.
[24] International Rectifier, "Current ratings of power semiconductors and thermal design," Application Note AN-949, Jul. 2012.

Karthik A received the B.Tech. degree from Kerala University, Trivandrum, India, and the M.Sc. (Eng.) degree from the Center for Electronics Design and Technology (CEDT), Indian Institute of Science (IISc), Bangalore, India, in 2008 and 2014, respectively.

He was previously a Project Engineer with the Strategic Electronics Group, Centre for Development of Advanced Computing, Trivandrum. He is currently at CEDT, IISc. His research interests include power conversion, energy management, control, and audio engineering.

Loganathan Umanand received the B.S. degree in electronics and communications from Bangalore University, Bangalore, India, in 1987, and the M.Tech. degree in electronics design and the Ph.D. degree from the Center for Electronics Design and Technology (CEDT), Indian Institute of Science (IISc), Bangalore, in 1989 and 1996, respectively.

His Ph.D. dissertation was in the area of control for high-performance induction motors drives. He is currently an Associate Professor at CEDT, IISc. His major research interests include photovoltaic system design, bond graph modeling of power electronic systems, high-performance control of induction motors, designing for reliability, and hybrid electric vehicles.